

Morphological and Mechanical Properties of Hydroxyapatite Bilayer Coatings Deposited on 316L SS by Sol–Gel Method



DJAHIDA SIDANE, HAFIT KHIREDDINE, SABEHA YALA, SALIMA ZIANI, FATIMA BIR, and DIDIER CHICOT

The present paper reports on the influence of the addition of TiO_2 and SiO_2 oxides as sub-layer, on the morphological and mechanical properties of the hydroxyapatite (HAP) bioceramic coatings deposited on 316L stainless steel by sol–gel method in order to improve the properties of hydroxyapatite and expand its clinical application. The stability of the sols suspensions was evaluated by measuring the time dependence of the viscosity. Annealed properties of the coatings were analyzed by XPS, XRD, SEM, and EDS. The Vickers microhardness of the coatings is obtained under the same indentation load of 10 g. The hydroxyapatite coating deposited on the surface of the 316L SS substrate exhibits a porous carbonated apatitic structure. The results clearly demonstrate that HAP- TiO_2 and HAP- SiO_2 bilayer coatings where hydroxyapatite is deposited on the surface of TiO_2 - and SiO_2 -coated 316L SS substrate systems were highly homogeneous and uniform and show higher microhardness compared to HAP-coated 316L SS. A gap of nearly 10 pct is observed. The addition of TiO_2 and SiO_2 as sub-layer of a hydroxyapatite coating results in changes in surface morphology as well as an increase of the microhardness.

DOI: 10.1007/s11663-015-0397-8

© The Minerals, Metals & Materials Society and ASM International 2015

I. INTRODUCTION

DUE to its chemical and structural similarities with the mineral phase of bone and teeth, synthetic hydroxyapatite, $\text{Ca}_{10}(\text{PO}_4)_6(\text{OH})_2$, HAP, is widely used for hard tissues repair. One of the most important requirements of a material designed for bone substitution and/or repair, is the ability to create a bond with the host living bone.^[1]

The sol–gel dip coating process is easily applicable to surface coating, and it allows the preparation of high-quality HAP thin films on metal substrates.^[2,3] Moreover, it has been reported that the materials prepared by sol–gel deposition are more bioactive than those prepared by other methods.^[4,5] In order to deposit biomedical coatings with a defined surface structure and morphology, the chemical, structural, and morphological properties of synthetic HAP can be modulated by changing the conditions of synthesis. At the solution preparation stage of the sol–gel process, the major concern involves the aging effect that influences subse-

quent microstructural evolution of sol–gel derived coatings.^[6–9] Many recent studies have investigated the variation of the microstructural, compositional, morphological, and surface properties of the hydroxyapatite coatings with the influence of the reinforcing process such as the addition of titania phase in order to improve the bioactivity, mechanical, and bonding strength of the nanocomposite coatings developed.^[10–13] Thin films of titania coating on 316L SS possess combined advantages of biocompatibility and corrosion-resistant properties.^[14] Moreover, it is recognized that silica-based sol–gel systems usually have a high content of surface silanol groups, which have been reported to promote *in vitro* and *in vivo* nucleation of apatite.^[15]

In this paper, we propose a strategy for obtaining different morphological HAP coatings containing TiO_2 and/or SiO_2 oxides ceramic materials.

As a simple and direct measurement, indentation hardness is often used as an initial guideline for the qualification of a coating for any application requiring wear resistance. As a rule of thumb, intrinsic film hardness can be directly measured when the penetration depth of the indenter is lower than 10 pct of the coating thickness. In this case, the substrate is supposed to not interfere in the hardness measurement. This assumption is at least valid for hard films on soft substrates but has to be verified for soft films on hard substrates. For the recent generation of coatings that are becoming thinner and thinner, very often below than 4–5 μm , this rule of thumb is sometimes difficult to be respected mainly in microindentation.^[16,17]

DJAHIDA SIDANE, SABEHA YALA, and FATIMA BIR, Doctoral Students, HAFIT KHIREDDINE, Professor, and SALIMA ZIANI, Assistant Professor, are with the Laboratoire de Génie de l'Environnement, Département de Génie des Procédés, Université de Bejaia, Route Targa Ouzemour, 06000 Bejaia, Algeria. Contact e-mail: dj.sidane@yahoo.fr DIDIER CHICOT, Professor, is with the Laboratoire de Mécanique de Lille (LML), UMR CNRS 8107, Université des Sciences et Technologie de Lille 1, IUT Le Recueil, Rue de la Recherche, BP 90179, 59653 Villeneuve d'Ascq Cedex, France.

Manuscript submitted January 15, 2015.

Article published online June 24, 2015.

II. EXPERIMENTAL METHODS AND MATERIALS

Defined amounts of phosphorus pentoxide (P_2O_5 , Prolabo 100 pct) and calcium nitrate tetrahydrate ($Ca(NO_3)_2 \cdot 4H_2O$, Fluka 98 pct) were dissolved in absolute ethanol, to form solutions with concentrations of 0.5 and 1.67 mol/l, respectively. The two solutions were mixed and this results in the formation of a HAP sol having Ca/P molar ratio of 1.67.^[7] The mixture was continuously stirred at ambient temperature for 24 hours. This produces translucent sol.

Titanium isopropoxide (TIP, Fluka 100 pct) was used as a titania precursor in the sol-gel process. The reactivity toward water is modified by acetic acid (HOAc) (molar ratio of TIP/HOAc = 1/10) which is also used as catalyst. 2-Methoxy ethanol was added to adjust the degree of viscosity of the solution. This solution with titanium molar concentration of approximately 0.47 M was vigorously stirred under ambient temperature conditions.^[18]

Silica sol-gel solution was obtained by mixing tetraethylorthosilicate (TEOS, Fluka 98 pct) and methyltriethoxysilane (MTES, Fluka 98 pct) in equimolar ratio. Hydrochloric acid (0.1 N) and acetic acid (HOAc) were added as catalysts, their role is to increase the hydrolysis and condensation. The reaction rate of the mixture ($H_2O + HOAc$)/(TEOS + MTES) was 1.7.^[19] After stirring the solution, under ambient temperature conditions, a transparent viscous sol was obtained.

316L SS substrates of $20 \times 10 \times 5$ mm sample size were mechanically polished using different silicon carbide grit papers up to #1200 grades. Final polishing was done using diamond paste ($2 \mu m$) and ($0.7 \mu m$) to produce scratch-free mirror finish surface. The substrates were ultrasonically degreased with acetone and washed with running double distilled water. Finally, they were dried at 423 K (150 °C) for 10 minutes.

The TiO_2 coatings were obtained by dipping the polished, washed, and dried metal substrates in the suspension with dipping rate of 20 mm/min and annealed at the temperature of 723 K (450 °C) for 60 minutes. The SiO_2 coatings were deposited on the surface of the substrates with dipping rate of 100 mm/min and annealed at the temperature of 773 K (500 °C) for 60 minutes. The HAP- TiO_2 bilayer coatings were obtained by the deposition of the hydroxyapatite on the outer surface of the TiO_2 single coatings, with dipping rate of 80 mm/min and annealed at the temperature of 773 K (500 °C) for 60 minutes; in the same way, the HAP- SiO_2 bilayer coatings were obtained by the deposition of the hydroxyapatite on the outer surface of the SiO_2 single coatings. The HAP single coating was also deposited on the surface of the substrate to be compared with the bilayer coating features.

In order to analyze the effect of aging on the formation of gel, each sol (HAP, TiO_2 , and SiO_2) was divided into 3 parts and kept closely capped for 24, 48, and 72 hours, at the ambient temperature, the TiO_2 sol was also maintained at 373 K (100 °C) for 24 hours. The pH measurements (Ultra BASIC pH Meter) and the

rheological measurements using a rotational rheometer (VT 500/501 Haake, Mess-Technik.Gmbhu) of the sols were continuously monitored throughout the aging period. Phase composition of the coatings were analyzed by X-ray diffraction (XRD) (Panalytical type MPD) using $CuK\alpha$ radiation in the range of $20 < 2\theta < 80$ deg. The chemical states of the coatings were characterized by X-ray photoelectron spectroscopy (XPS) with a Thermo L-alpha spectrometer, using monochromatized Al $K\alpha$ radiation as the excitation source ($h\nu = 1486.6$ eV), collected at 0 deg from the surface normal and detected with a hemispherical analyzer. The spot size of the XPS source on the sample is about 200 μm , and the pass energy was set at 20 eV. During data acquisition pressure is kept below (1×10^{-9} Torr). Spectra are fitted using a 70/30 pct linear combination of Gaussian and Lorentzian profiles. Peak positions obtained after analysis are found essentially constant (± 0.3 eV). The morphology and the elemental analysis of the surface of the coated specimen were performed using scanning electron microscopy (SEM QUANTA 200, detector SUTW-Sapphire). The thickness of the coating layer was measured using a profilometry analysis "DEKTAK 150 SURFACE PROFILER," by scanning the surface of the coating at an interval of 1000-8000 μm . Three different areas were scanned and measured to determine the mean thickness.

Vickers microhardness indentations were performed using a Zwick microhardness machine (ZHV10) with a dwell time of 15 seconds applied at the maximum indentation load. To analyze the homogeneity and the indentation size effect (hardness-load dependence) of the substrate, a series of indentation loads ranging between 10 and 200 g were performed. Hardness of the coatings is determined under the lowest indentation load available on the instrument, *i.e.*, 10 g, to minimize the influence of the substrate on the hardness measurement. The hardness value was the result of 10 indents measurement to be representative. In this study, the objective of the mechanical analysis is to estimate and compare the hardness gap due to the modification of the coating structure.

III. RESULTS AND DISCUSSION

A. Aging Effect on the Rheological Properties of Sols

The viscosity of the HAP, titania, and silica sols was analyzed and evaluated as a function of aging time, *i.e.* 24, 48, and 72 hours, under ambient conditions. The viscosity of the TiO_2 sol aged for 24 hours at 373 K (100 °C) was considered too. It is known that the amount of the solution acquired by the substrate for dip coating deposition depends on the solution viscosity. The coefficients of viscosity are presented in Table I jointly to the pH measurement. The reference number in brackets refers to the aging time (Table I).

It can be seen in Table I that the pH vs time continuously decreases for each sol. The viscosity of the HAP and TiO_2 sols, aged at the ambient temperature, varies slightly with aging time. From visual

Table I. pH and Viscosity Measurements of the HAP, TiO₂, and SiO₂ Sols

Sol (test N°)	Time (h)	pH	Viscosity (mPa s)
HAP (1)	24	0.70	5.22
HAP (2)	48	0.62	5.49
HAP (3)	72	0.59	5.95 at ambient temperature
TiO ₂ (1)	24	2.46	5.46
TiO ₂ (2)	48	2.44	5.99
TiO ₂ (3)	72	2.17	5.99 at ambient temperature
TiO ₂ (1)	24	2.22	7.96 at $T = 373$ K (100 °C)
SiO ₂ (1)	24	0.97	6.33
SiO ₂ (2)	48	0.88	25.70
SiO ₂ (3)	72	—	gel at ambient temperature

observations, the sols were indistinguishable from each other, regardless the aging period. They were stable and no gelation occurred over an aging period as long as several days. This is consistent with observations by Livage *et al.*,^[20] whom attributed this stability to a limited degree of polymerization. The desirable solid structure depends mainly on the degree of viscosity. Liu *et al.*^[21] indicate that aging of the precursor solution has been found to be critical in developing an apatitic phase and specific aging time period either at ambient or higher temperature is necessary to form a phase-pure apatite. In the case of the TiO₂ sol maintained at 373 K (100 °C) for 24 hours, there is a significant increase in the viscosity coefficient which can be attributed to the aging effect at higher temperature [373 K (100 °C)] that accelerates the hydrolysis and polymerization reactions. The effect of the temperature of aging on the formation of the TiO₂ films can be seen in Figures 1(a) and (b). The aging effect at the temperature of 373 K (100 °C) plays an important role on the formation of TiO₂ coating. While in the case of the silica sols, aged at ambient temperature, the increase in the viscosity coefficient is attributed to the addition of the mineral acid in the sol preparation that accelerates the hydrolysis and polymerization reactions during the aging process. Here there is no influence of the temperature of aging and the SiO₂ coating (see Figure 1(c)) was prepared from the sol aged for 24 hours at ambient temperature.

B. Morphology of the SiO₂- and TiO₂-Deposited Single Coatings

Figures 1(a) and (b) show the surface of the TiO₂ coatings prepared with two different sols. The TiO₂ coating presented in Figures 1(a) prepared from the sol aged for 24 hours at the ambient temperature, deposited with dipping rate of 20 mm/min, and annealed at 723 K (450 °C)/60 min, shows a fractured structure at the surface that leads to the production of a number of islands. According to Xu *et al.*^[22], this mechanism is beneficial to the adhesive strength between TiO₂ and HAP layers, because the HAP gel can fill into the cracks and cover the surface of TiO₂ film. While the TiO₂ coating prepared from the sol aged for 24 hours at the

temperature of 373 K (100 °C), deposited with dipping rate of 20 mm/min, and then annealed at 723 K (450 °C)/60 min, it shows a uniform surface (Figure 1(b)). The aging effect at higher temperature [373 K (100 °C)] is a critical stage of the TiO₂ sol synthesis, influencing subsequent microstructural evolution of sol-gel, consequently the nature of the TiO₂ coating obtained. The structure becomes quite compact and homogeneous, which is in agreement with the results of Balamurugan *et al.*^[18] Both types of coatings are very thin and transparent, they reveal the appearance of the substrate surface. Figure 1(c) shows the surface of the SiO₂ coating prepared from the sol aged for 24 hours at the ambient temperature, deposited with dipping rate of 100 mm/min, and then annealed at 773 K (500 °C)/60 min. As it can be seen, the sample shows the presence of some micro-pores and no visible cracks are detected.

C. XPS Analysis of SiO₂, TiO₂, and HAP Single Coatings

The XPS profiles shown in Figure 2 indicate the surface chemical compositions of the HAP, TiO₂, and SiO₂ coatings. The peak at 284.6 eV is assigned to the contaminated carbon. According to Zhang *et al.*^[23], carbon is only absorbed on the very outer surface of the films. Peak of Si2p at 103.07 eV is assigned to SiO₂. The peak of Ti2p at 459.29 eV is attributed to TiO₂. The peak of O1s is assigned to the generated oxide films. The XPS spectrum obtained on the surface of HAP indicates the existence of Ca, P, and O, the binding energy of Ca2p is 348.76 eV, which is consistent with the binding energy of HAP.^[23]

D. XRD Spectra of SiO₂, TiO₂, and HAP Single Coatings

In Figure 3, the XRD pattern for the HAP coating shows peak positions and widths, which correspond to a crystallized HAP structure (JCPDF no. 00-009-0432). The HAP characteristic triplet peaks at (211), (112), and (300) planes are observed for 2θ values between 31 and 33 deg. In the XRD pattern of the TiO₂ coating, all

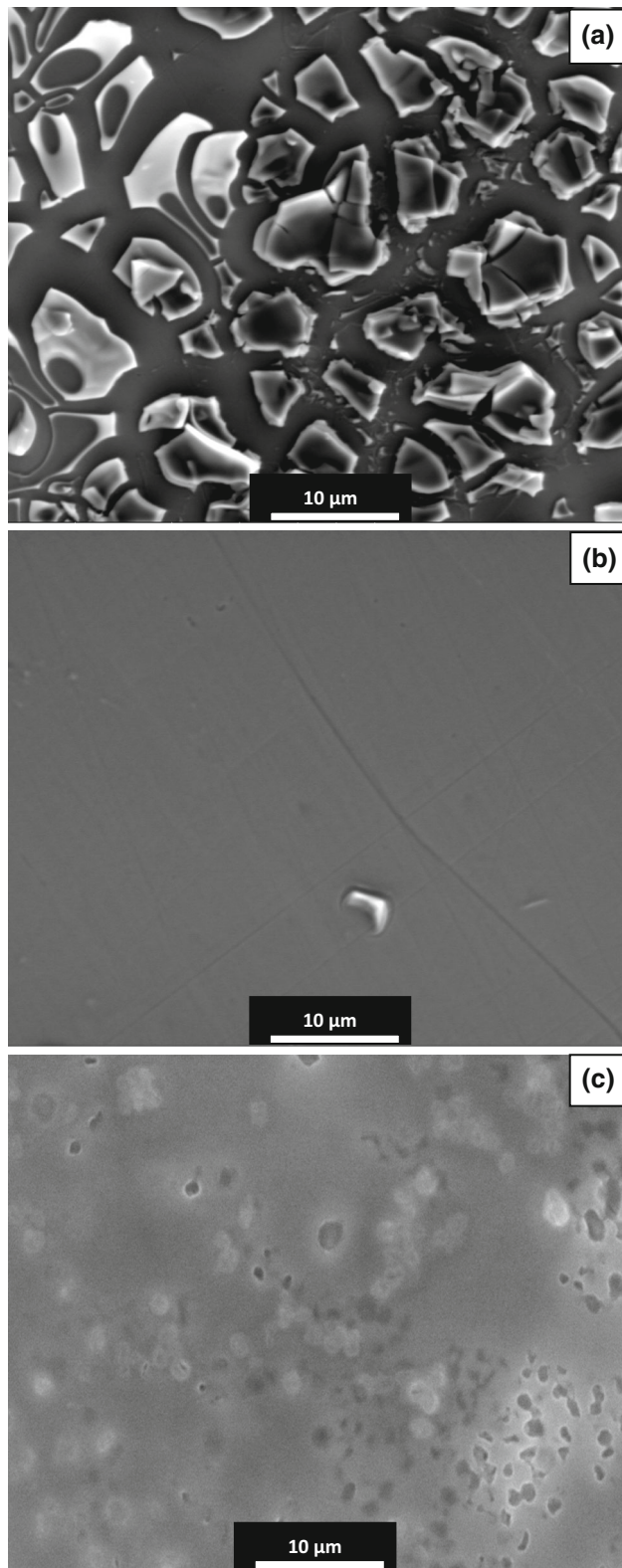


Fig. 1—SEM observations of the TiO₂ single coatings prepared from the sol aged for 24 h at (a) ambient temperature and (b) 373 K (100 °C), both coatings are deposited with dipping rate of 20 mm/min and annealed at 723 K (450 °C)/60 min. (c) SiO₂ single coating prepared from the sol aged for 24 h at ambient temperature, deposited with dipping rate of 100 mm/min, and annealed at 773 K (500 °C)/60 min.

peaks correspond to the TiO₂ phase besides the reflections from steel substrate. The XRD analysis reveals a crystalline structure of anatase (JCPDF no. 00-004-0477). In the XRD pattern of the SiO₂ coating surface, only, the phase of the substrate is observed. No crystalline phase of SiO₂ is detected by the X-rays diffraction. Here the SiO₂ sol-gel synthesized is in amorphous state. Then it can be compared to the silica gel which has amorphous and porous structure. XRD pattern of the silica powder before and after annealing at the temperature of 773 K (500 °C) for 60 minutes is given in Figures 4(a) and (b), respectively. There is no crystalline phase of SiO₂ detected by the X-rays diffraction, the powder is amorphous.

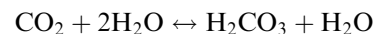
E. Effect of TiO₂, SiO₂ Inner Layers

1. Morphology of the HAP single and HAP-SiO₂, HAP-TiO₂ bilayer coatings

Figure 5 collects the SEM images related to the HAP single coating (Figure 5(a)) and bilayer coatings (Figure 5b—HAP-TiO₂ and Figure 5(c)—HAP-SiO₂). The HAP single coating exhibited a porous surface composed of spherical agglomerates. According to Feng *et al.*^[24] and Rajabi-Zamani *et al.*,^[25] the agglomerated structure is due to the aging period. Pores having a spherical shape were sparsely distributed on the coating surface. The morphological feature of the HAP-TiO₂ bilayer coating is shown in Figure 5(b). The surface appears dense and uniform. SEM surface examination reveals no detectable cracks and absence of pores for these coatings. The surface features of the TiO₂ underlying film (Figure 1(b)) appear to be replicated by the surface of the HAP outer layer. Figure 5(c) is related to the HAP-SiO₂ bilayer coating in which the SiO₂ base film used is illustrated in Figure 1(c). The surface morphology of the HAP-SiO₂ coating is homogenous, the pores still exist, since the SiO₂ underlying structure is porous, but they are reduced compared to the HAP single coating (Figure 5(a)).

2. Elemental analysis of the HAP single and HAP-TiO₂, HAP-SiO₂ bilayer coatings

The EDS spectrum of the HAP coating is shown in Figure 6(a). It indicates the elemental composition of the HAP. Intense bands for Ca, P, and O are obtained with small peaks corresponding to Fe and Cr, present into the substrate. In addition, EDS spectrum indicates the presence of the carbon peak. According to Yala *et al.*^[26] who synthesized the hydroxyapatite using a similar sol-gel processing route, the coatings can be considered as a carbonated apatite. The presence of the carbonate group in the apatite structure corresponds to partial substitution of phosphate ions (B site) by carbonate ions.^[27] The source of the carbonate was probably due to the absorption of atmospheric CO₂ into the ethanolic solution. Carbonate ion is produced by the reaction of CO₂ with water and OH⁻ as follows^[28]:



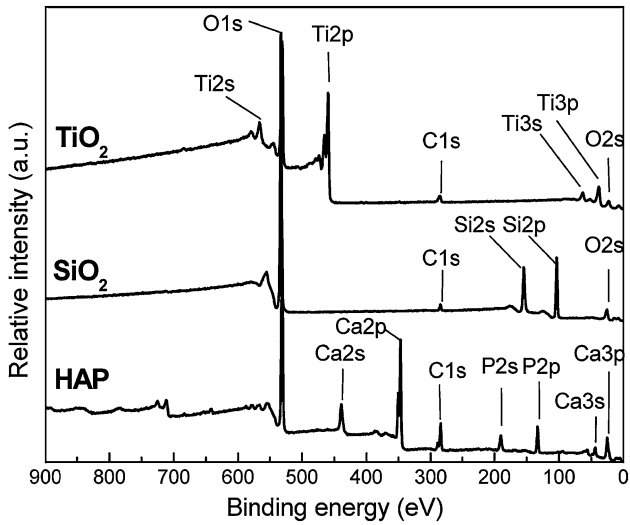


Fig. 2—XPS spectra of the TiO₂, SiO₂, and HAP single coatings. HAP is deposited with dipping rate of 80 mm/min and annealed at 773 K (500 °C)/60 min.

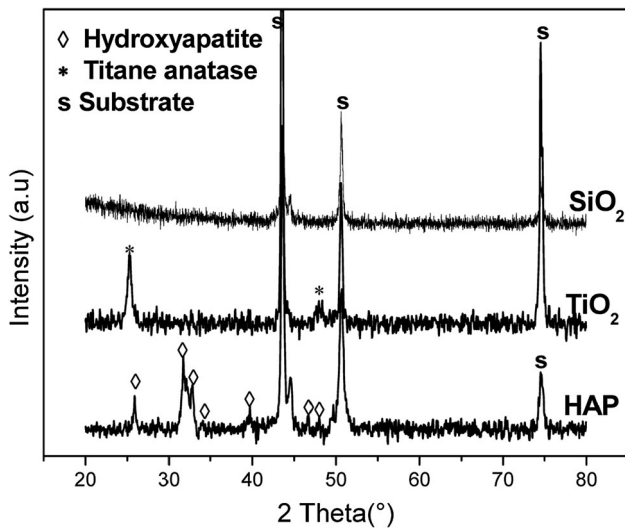
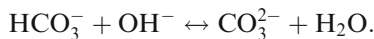
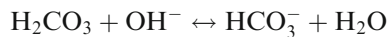


Fig. 3—XRD patterns of the SiO₂, TiO₂, and HAP single coatings.



EDS spectra of the HAP-TiO₂ and HAP-SiO₂ bilayer coatings are shown in Figures 6(b) and (c), respectively. EDS analysis clearly illustrated the presence of HAP, TiO₂, and SiO₂ elements on the substrate.

3. XRD analysis of the HAP-TiO₂ and HAP-SiO₂ bilayer coatings

XRD patterns of the HAP-TiO₂ and HAP-SiO₂ bilayer coatings are shown in Figure 7. The diffraction spectrum observed for the HAP-TiO₂ coating is given in

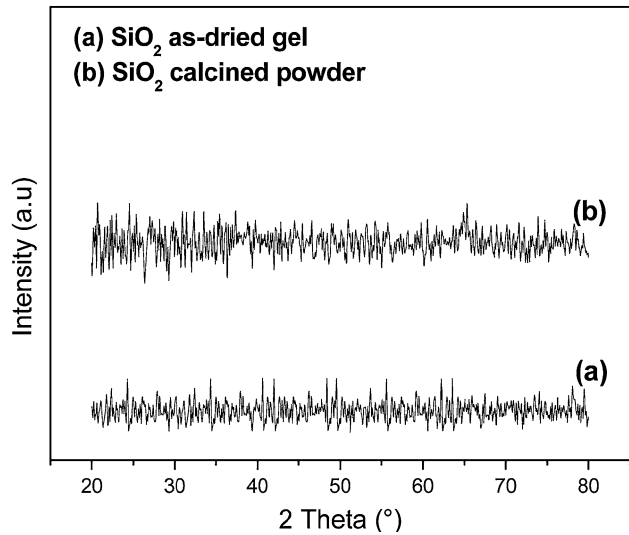


Fig. 4—XRD patterns of the (a) SiO₂ as-dried gel and (b) SiO₂ calcined powder at 773 K (500 °C)/60 min.

Figure 7(a). It consists of sharp peaks attributed to the 316L SS substrate and several major peaks are corresponding to HAP structure. In addition, the XRD pattern reveals the crystalline structure of anatase corresponding to the existing TiO₂ phase. XRD pattern of the HAP-SiO₂ coating surface is exposed in Figure 7(b). The major phases of HAP and the substrate are observed. No crystalline phase of SiO₂ is detected. As it is demonstrated above, the SiO₂ phase is in amorphous state. It can be seen from Figure 7(a) that the HAP peaks become more distinct and, also the widths of the peaks become more narrow, when the HAP is deposited on the surface of the TiO₂ crystalline coating, that suggests an increase in the degree of crystallinity compared to the HAP deposited on the surface of the SiO₂ amorphous coating (Figure 7(b)). When compared to the EDS analysis realized on these coatings, it can be deduced that the combinations of HAP-TiO₂ layers and HAP-SiO₂ layers were produced.

F. Microhardness Analysis

In this work, the mechanical characterization of the coated systems is only focused on the hardness gap due to the presence of HAP coating and to the addition of the inner layers of oxides. Further works on the mechanical properties determination are ongoing by means of nanoindentation experiments. Such scale of measurement will allow determining the elastic modulus and the hardness by applying the methodology of Oliver and Pharr.^[29]

Vickers hardness experiments were performed on the substrate before deposition. The Vickers hardness of the stainless steel substrate was measured in the load range of 10-200 g. Table II gives the hardness number computation for each indentation load. As it can be seen, the microhardness of the substrate varies according to the applied load between 133 and 168 HVN. These fluctuations can be the result of three parameters: (i) the

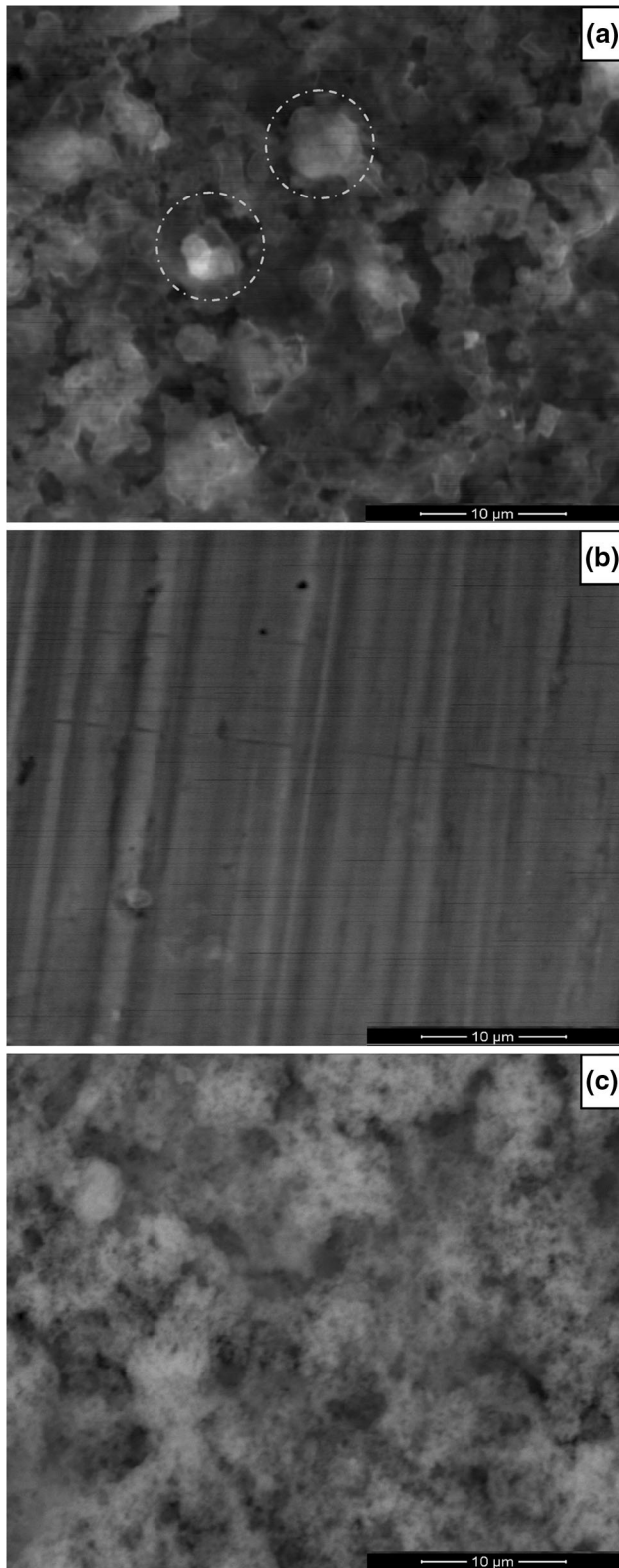


Fig. 5—SEM observations of the (a) HAP single coating, the white circles inserted indicate the spherical agglomerates, (b) HAP-TiO₂ bilayer coating and (c) HAP-SiO₂ bilayer coating.

microstructure heterogeneity due to the grain morphology (size and distribution in relation to the indent position), (ii) the volume of the plastic zone which

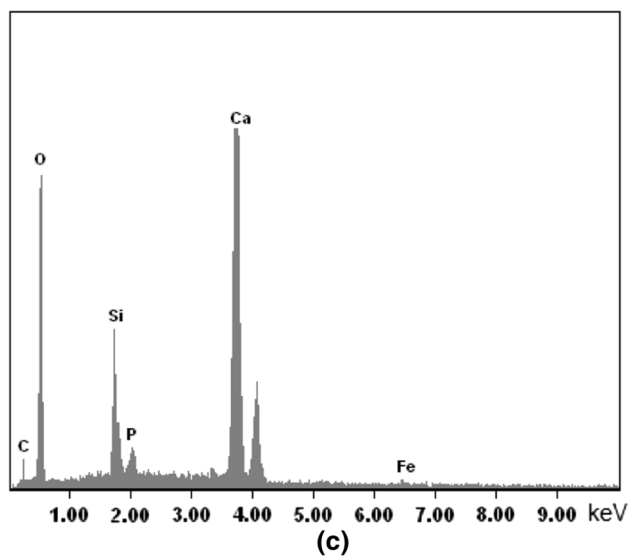
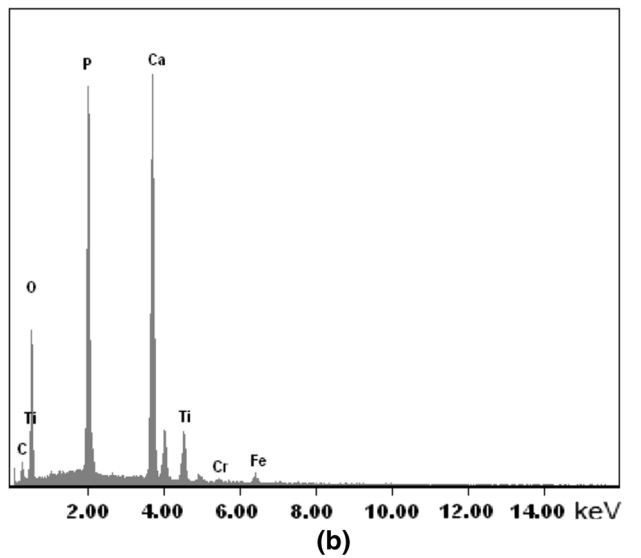
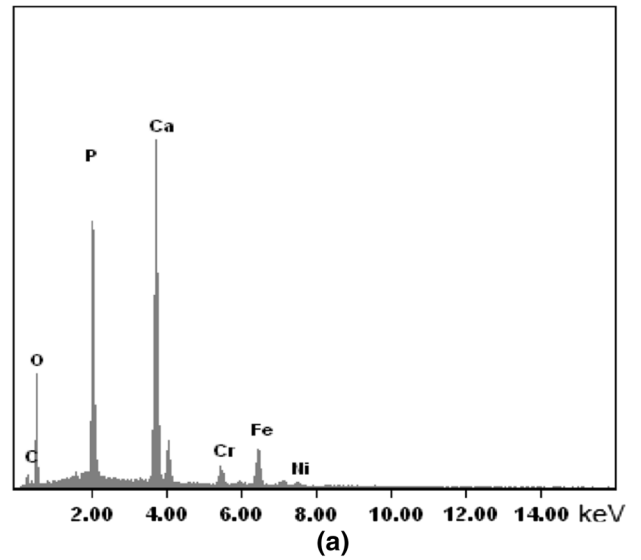


Fig. 6—EDS analysis of (a) HAP single coating, (b) HAP-TiO₂ and (c) HAP-SiO₂ bilayer coatings.

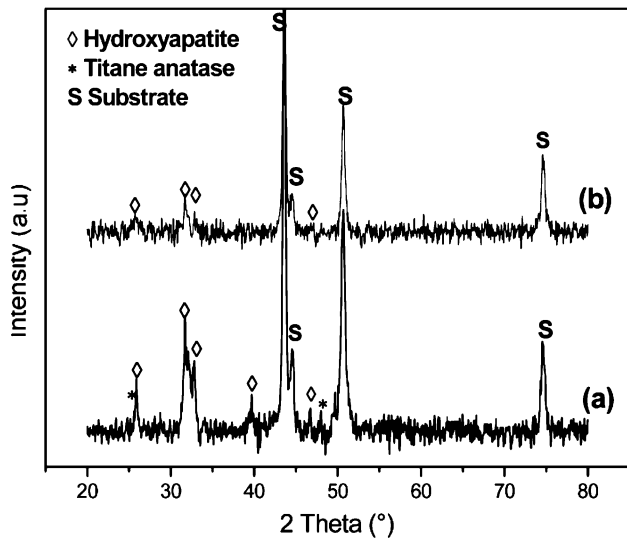


Fig. 7—XRD patterns of the (a) HAP-TiO₂ and (b) HAP-SiO₂ bilayer coatings.

depends on the applied load (notion of VER—volume elementary of reference), and (iii) the hardness-load dependence which is usually represented by an increase of the hardness number with the decrease of the indentation load^[30] (it can be due to various parameters like the work hardening by polishing, dislocation network, *etc.*). On the other hand, even if Table II shows a slight variation of the Vickers hardness with the load, the hardness values are close enough to consider a mean value, *i.e.*, 150 HV for the substrate hardness. For characterizing the hardness of the coatings, only indentation experiments using the indentation load of 10 g have been performed. The comparison between the different coatings is acceptable since their coating thicknesses are quite similar, around 2 μm. In this condition, 10 indents have been performed on each coating and Table III collects the average value of the indent diagonal and the corresponding Vickers hardness number. It is clear that at such low indentation load and by using the optical device of a classical instrument, the standard deviations are inevitably quite important as much as the sizes of the indents are lower than 10 μm.

Independently on the crack initiation around the indent for which their influence on the hardness measurement is not well known, the hardness calculation of the coated systems have been performed neglecting the influence of the cracks network. As mentioned in Table III, the Vickers hardness values are close enough to consider no significant influence of the inner layers on the global hardness measurement. In addition, the indent diagonal which is around 9 μm corresponds to an indentation depth of 1.3 μm. This can be calculated considering geometrical relations accordingly to the specific shape of the Vickers indenter (136 deg being the half-angle between two opposite faces of the pyramidal indenter). Consequently, the relation between the diagonal, *d*, and the depth, *h*, for a Vickers indenter is often reduced to $d = h/7$. This allows verifying the tenth rule. As it is clear, the tenth rule is not respected since the

Table II. Experimental Data of the 316L SS Substrate as a Function of the Applied Load

Load (g)	10	20	50	150	200
Hardness (HVN)	155	168	150	149	133

Table III. Indent Diagonals and Vickers Hardness Number Obtained on the Different Coatings by Applying the Same Indentation Load of 10 g

Coating	HAP	HAP-TiO ₂	HAP-SiO ₂
Diagonal (μm)	9.3 ± 0.2	8.9 ± 0.3	9.0 ± 0.4
Hardness (HVN)	215 ± 10	235 ± 16	230 ± 20

indenter penetration is much higher than 10 pct of the coating thickness close to 2 μm. In practice, the penetration depth must be lower than 0.2 μm, whereas it is equal to 1.3 μm. As a result, the hardness value indicated in Table III is a composite hardness taking into account a part of the elasto-plastic response of the substrate.^[31] In order to estimate the apparent hardness of the coating, the model of Jönsson and Hogmark^[32] is the only model applicable because the calculation has been performed under only one indentation load. This model, which is predictive and not descriptive since all the involved parameters are known, expresses the composite hardness, H_C , as a function of the hardness of the substrate, H_S , and that of the film, H_F , as follows:

$$H_C = H_S + a \cdot (H_F - H_S), \quad [1]$$

where *a* is the parameter representing the influence of the film in the hardness measurement.

For Jönsson and Hogmark,^[32] this parameter can be expressed as a function of the indent diagonal, *d*, and the coating thickness, *t*, as follows:

$$a = \frac{2Ct}{d} - \left(\frac{Ct}{d}\right)^2, \quad [2]$$

where *C* is a constant equals to 0.5 for brittle materials which is the case here since cracks have been observed around the indents in the coatings.

Considering $t = 2 \mu\text{m}$, the average diagonal value of 9 μm for *d* and the constant *C* equals to 0.5, the computation of the parameter *a* leads to 0.21. Applied to Eq. [1] using the hardness value of the substrate of 150 HV and the hardness value of the composite of 230 for the bilayer HAP-TiO₂, HAP-SiO₂ coatings and 215 HV for the HAP coating, the approximate Vickers hardness number of the separate coating is found to be close to 530 HV for the bilayer HAP-TiO₂, HAP-SiO₂ coatings, and 459 HV for the HAP coating. A gap of nearly 10 pct is observed. This result is interesting but it must be verified by nanoindentation employing the continuous stiffness measurement method. Indeed, this methodology will be necessary to separate the contribution of each layer in the composite coatings.^[33–35]

IV. CONCLUSIONS

The sol-gel dip coating technique described in the present investigation has the advantage of producing ceramic coatings at low temperature. Layered surfaces including HAP, TiO₂, and SiO₂ coatings on the 316L SS metallic implant have been used. Combinations of HAP-TiO₂ layers and HAP-SiO₂ layers were produced. The surface of HAP-TiO₂ bilayer coating is uniform and the HAP-SiO₂ surface shows a homogenous structure. While the surface of HAP single coating is porous and presents some aggregations. As a conclusion, the morphology of the resulting bilayer coatings is dependent on the surface features of the underlying oxide layers. So the deposition of the inner layers provide the formation of new types of hydroxyapatite coatings at the same condition of annealing [773 K (500 °C)/60 min]. This represents an advantage for the various applications of the hydroxyapatite bioceramic in the medical field. Classical hardness measurements conducted on the coated systems under the same indentation load (10 g) indicates that the microhardness of the HAP coating is improved by the addition of TiO₂ and SiO₂ inner layers on the 316L SS substrate. However, further deeper analysis of the mechanical properties of these coatings is required to improve our knowledge of the mechanical properties of each layer constituting the coated system.

ACKNOWLEDGMENTS

The authors gratefully acknowledge the contribution of Prof. Abdelaziz Ati, from the mechanical laboratory of Bejaia for providing the mechanical experiments.

REFERENCES

1. T. Kokubo, H.M. Kim, and M. Kawashita: *Biomaterials*, 2003, vol. 24, pp. 2161–75.
2. D.M. Liu, T. Troczynski, and W.J. Tseng: *Biomaterials*, 2001, vol. 22, pp. 1721–30.
3. A. Montenero, G. Gnappi, F. Ferrari, M. Cesari, E. Salvioli, L. Mattogno, S. Kaciulis, and M. Fini: *Mater. Sci.*, 2000, vol. 35, pp. 2791–97.
4. P. Li and K. De Groot: *J. Sol-Gel. Sci. Technol.*, 1994, vol. 2, pp. 797–801.
5. D.B. Haddow, P.F. James, and R. Noort: *J. Mater. Sci. Mater. Med.*, 1996, vol. 154, pp. 255–60.
6. F.A.K. Azem and A. Cakir: *J. Sol-Gel. Sci. Technol.*, 2009, vol. 51, pp. 190–97.
7. S. Kim and P.N. Kumta: *Mater. Sci. Eng., B*, 2004, vol. 111, pp. 232–36.
8. A. Balamurugan, S. Kannan, and S. Rajeswari: *Can. Metall. Q.*, 2004, vol. 43, pp. 293–96.
9. A. Balamurugan, G. Balossier, and S. Kannan: *Mater. Lett.*, 2006, vol. 60, pp. 2288–93.
10. A.J. Nathanael, N.S. Arul, N. Ponpandian, D. Mangalaraj, and P.C. Chen: *Thin Solid Films*, 2010, vol. 518, pp. 7333–38.
11. A.J. Nathanael, D. Mangalaraj, and N. Ponpandian: *Compos Scie Technol*, 2010, vol. 70, pp. 1645–51.
12. C.C. Yang, C.Y. Huang, C.C. Lin, and S.K. Yen: *J. Electrochem. Soc.*, 2011, vol. 158, pp. 13–20.
13. A.J. Nathanael, J.H. Lee, and S.I. Hong: *Adv. Sci. Lett.*, 2012, vol. 15, pp. 285–90.
14. J. Blum, K.L. Eckert, A. Schroeder, M. Petitmermet, S.W. Ha, and E. Wintermantel: in *Bioceramics*, T. Kokubo, T. Nakamura, and F. Miyaji, eds., Pergamon, Otsu, 1996, pp. 89–92.
15. P. Li, C. Ohtsuki, T. Kokubo, K. Nakanishi, N. Soga, T. Nakamura, and T. Yamamuro: *J. Am. Ceram. Soc.*, 1992, vol. 75, pp. 2094–97.
16. D.E. Kramer, A.A. Volinsky, N.R. Moody, and W.W. Gerberich: *J. Mater. Res.*, 2001, vol. 16, pp. 3150–57.
17. A.C. Fischer-Cripps: *Vacuum*, 2000, vol. 58, pp. 569–85.
18. A. Balamurugan, S. Kannan, and S. Rajeswari: *Mater. Lett.*, 2005, vol. 59, pp. 3138–43.
19. P. Galliano, J.J. Damborenea, M. Pascual, and A. Duran: *J. Sol-Gel. Sci. Technol.*, 1998, vol. 13, pp. 723–27.
20. J. Livage, P. Barboax, M.T. Vandendorre, C. Sichmutz, and F. Taulelle: *J. Non-Cryst. Solids*, 1992, vols. 147–148, pp. 18–23.
21. D.M. Liu, T. Troczynski, and W.J. Tseng: *Biomaterials*, 2002, vol. 23, pp. 1227–36.
22. W. Xu, W. Hu, M. Li, and C. Wen: *Mater. Lett.*, 2006, vol. 60, pp. 1575–78.
23. W. Zhang, C. Wang, and W. Liu: *Wear*, 2006, vol. 260, pp. 379–86.
24. W. Feng, L. Mu-sen, L. Yu-peng, and Q. Yong-xin: *Mater. Lett.*, 2005, vol. 59, pp. 916–19.
25. A.H. Rajabi-Zamani, A. Behnamghader, and A. Kazemzadeh: *Mater. Sci. Eng., C*, 2008, vol. 28, pp. 1326–29.
26. S. Yala, H. Khireddine, D. Sidane, S. Ziani, and F. Bir: *J. Mater. Sci.*, 2013, vol. 48, pp. 7215–23.
27. J.F. Lafon: Thèse d'état, Ecole Doctorale Science-Technologie-Santé, Université de LIMOGES, 2004.
28. O.C. Wilson, Jr. and R.E. Riman: *J. Colloid Interface Sci.*, 1994, vol. 167, pp. 358–70.
29. W.C. Oliver and G.M. Pharr: *J. Mater. Res.*, 1992, vol. 7, pp. 1564–83.
30. D. Chicot, F. Roudet, A. Soom, and J. Lesage: *Surf. Eng.*, 2007, vol. 23, pp. 32–39.
31. D. Chicot, E. Bemporad, G. Galtieri, F. Roudet, M. Alvisi, and J. Lesage: *Thin Solid Films*, 2008, vol. 516, pp. 1964–71.
32. B. Jönsson and S. Hogmark: *Thin Solid Films*, 1984, vol. 114, pp. 257–69.
33. K. Zeng and C.H. Chiu: *Acta Mater.*, 2001, vol. 49, pp. 3539–51.
34. B. Wolf, A. Richter, and V. Weinhacht: *Surf. Coat. Technol.*, 2004, vol. 183, pp. 141–50.
35. J. Musil, F. Kunc, H. Zeman, and H. Poláková: *Surf. Coat. Technol.*, 2002, vol. 154, pp. 304–13.